Lasers in Surgery and Medicine 34:174–181 (2004)

Characterization of Port Wine Stain Skin Erythema and Melanin Content Using Cross-Polarized Diffuse Reflectance Imaging

Byungjo Jung, PhD, Bernard Choi, PhD, Anthony J. Durkin, PhD, Kristen M. Kelly, MD, and J. Stuart Nelson, MD, PhD
Beckman Laser Institute, Irvine, California 92612-1475

Background and Objectives: Objective methods to assess quantitatively port wine stain (PWS) blanching in response to laser therapy are needed to improve laser therapeutic outcome. Previous studies have attempted to assess objectively PWS color based on point measurement devices. To date, these approaches have typically been limited by a number of factors such as small test area and need for contact. To address these issues, a cross-polarized diffuse reflectance imaging system and color image analysis method has been developed to evaluate quantitatively erythema and melanin content in PWS skin.
Study Design/Materials and Methods: A cross-polarized diffuse reflectance system has been constructed to acquire high resolution digital images while minimizing artifacts such as glare, shadowing, and nonuniform illumination effects that can compromise image fidelity. Furthermore, an image analysis algorithm has also been developed to analyze normal and PWS skin in terms of CIEL*a*b* color space parameters. Using the algorithm, images of color space intensity, L*, and saturation, a*, indices have been calculated to extract quantitative metrics of melanin and erythema, respectively.
Results: Compared to the cross-polarized diffuse reflectance image, the a* index image enhanced the contrast in regions of high and low erythema and seems to have quasi correlation with the L* index image. In the presented PWS patient example, the relative a* index difference (Δa*) image showed less erythema in PWS skin after laser treatment when compared to pre-treatment values.
Conclusions: Our cross-polarized imaging system and color image analysis method is a simple, noncontact technique that can indirectly provide quantitative measurement of erythema and melanin content in PWS skin. Lasers Surg. Med. 34:174–181, 2004.

Key words: CIEL*a*b* color space; digital color image; port wine stain; polarization; spectral image

INTRODUCTION

Port wine stains (PWS) are congenital hypervascular cutaneous malformations that occur typically on the face and neck. PWS patients may experience physical and emotional disability due to facial asymmetry and deformity. Pulsed dye lasers (PDL) are used for the clinical management of PWS patients [1–6]. To destroy PWS blood vessels permanently, PDL light at 585 or 595 nm wavelengths is absorbed preferentially by hemoglobin and converted to heat, resulting in vessel injury. Therapeutic outcome varies in large part due to site-to-site and interpatient variability in the following skin characteristics: epidermal melanin absorption, PWS depth, and blood vessel size [4,7,8].

Previous studies have demonstrated that clinical judgment of PWS skin appearance before and after laser treatment is strongly correlated with skin erythema [9,10]. Commercial devices, such as reflectance spectrophotometers and tristimulus colorimeters, can provide quantitative information on skin erythema and melanin. A reflectance spectrophotometer emits light at green and red wavelengths for quantification of erythema and melanin content, respectively [9–14]. A photodetector detects the reflected light, and erythema and melanin indices are computed. Alternatively, the tristimulus colorimeter illuminates skin with white light and reflected light is detected by three filtered photodiodes sensitive to either red, green, or blue (RGB) light [11,14]. The RGB data is subsequently converted to the Commission Internationale de l'Eclairage (CIE) L*a*b* color space (Table 1), which consists of three values: L* describes the reflected light intensity and varies from 0 (e.g., black) to 100 (e.g., white); a* describes color saturation and varies from −60 for green to +60 for red; and b* also describes color saturation and varies from −60 for blue to +60 for yellow [15]. The three coordinate axes are orthogonal to one another (Fig. 1). Previous studies have shown that a* and L* values (Table 2) represent the degree of skin erythema (hemoglobin content) and the degree of skin pigmentation (melanin content), respectively [15–18].

Although these reflectance measurement techniques can provide valuable information on PWS skin erythema and melanin content, they are limited in usefulness by practical

Contract grant sponsor: Arnold and Mabel Beckman Fellows Program (to B.C. and A.J.D.); Contract grant sponsor: Dermatology Foundation (to K.M.K.); Contract grant sponsor: National Institutes of Health (to J.S.N.); Contract grant numbers: AR-43419, AR-47551. E-mail: bjung@laser.bli.uci.edu
Accepted 13 October 2003
Published online in Wiley InterScience (www.interscience.wiley.com).
DOI 10.1002/lsm.10242

TABLE 1. Color Range of Parameters in CIE L*a*b* Color Space

CIE parameters	Quantitative range
L* (light intensxity)	0 (black) to +100 (white)
a* (saturation)	−60 (green) to +60 (red)
b* (saturation)	−60 (blue) to +60 (yellow)

considerations such as small test area and potential skin blanching due to probe contact, average measurement on test area, and low reproducibility at the same site. An alternative technology is to use a digital camera based system, which offers advantages such as computer interface for near real time feedback, flexibility of measurement area selection, and noncontact technique, [19–23]. However, for a digital imaging system to provide meaningful results, several factors must be controlled, such as camera sensitivity, shutter speed, aperture size, magnification, and patient positioning for consistent image analysis. Although those factors might be controlled, image quality may be affected by glare, shadowing, nonuniform illumination, and environmental lighting.

To address these issues, we have developed a cross-polarized diffuse reflectance imaging system to provide a quantitative measurement of erythema and melanin content in PWS skin. An image analysis method is used to assess the degree of erythema and melanin in selected PWS regions. The utility of this system for quantitative assessment of the blanching response of PWS skin after laser therapy is presented.

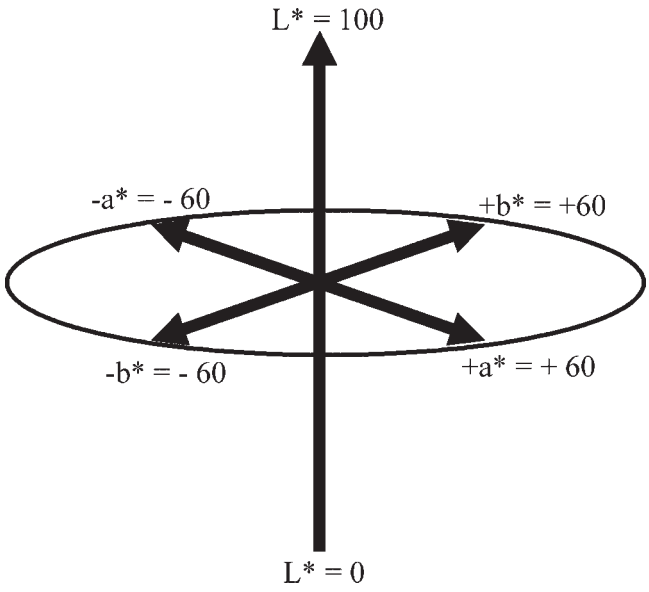

Fig. 1. Schematic of CIE L*a*b* color space. L* ranges from 0 (black) to 100 (white), a* from −60 (green) to +60 (red), and b* from −60 (blue) to +60 (yellow). Coordinate axes are orthogonal to each other.

TABLE 2. Definitions of L*, a*, and Δa*

Parameters	Definition
L*	Indicator of melanin content Higher value represents lower melanin content
a*	Indicator of erythema, which is directly related to hemoglobin content Higher value represents greater erythema
Δa*	Indicator of erythema difference between PWS and normal skin Positive values indicate that the region has greater erythema than the reference normal skin regions

MATERIALS AND METHODS

Cross-Polarized Diffuse Reflectance Imaging System

A digital color camera (Model DiMAGE7, Minolta Co., Osaka, Japan) was used to acquire images from PWS patients (Fig. 2a). The camera provided RGB images with 8 bits per color channel and sensor dimensions of 2,560 × 1,920 pixels. A macro ring flash (Model 1200, Minolta Co., Osaka, Japan) controlled by a flash controller provided shadow less, uniform illumination. To reduce glare caused by specular reflectance from the skin surface, a linear polarizer (Model A45-669, Edmund Industrial Optics, Barrington, NJ) was placed in front of the macro ring flash; a second identical polarizer (analyzer) was placed in front of the camera lens. Both were positioned such that their polarization axes were orthogonal. Camera output was displayed on a 9 inch color monitor (Model PR 0935B, Philips Magnavox, Atlanta, GA). A remote camera switch (Model RC-1000S, Minolta Co.) triggered image acquisition. To eliminate artifacts induced by environmental lighting, digital images were acquired in the dark. Camera settings (shutter speed: 1/60 second, aperture size: F/8) were identical for all acquired images. To ensure that test sites identified on the skin were positioned in a reproducible manner, a custom device (Fig. 2b) consisting of head and chin rests mounted on a rotary stage allowed for subject positioning at angles between 0° (front profile) and 90° (side profile).

In Vivo Imaging of PWS Skin

Digital images were acquired from a patient undergoing laser therapy at Beckman Laser Institute for a PWS on the right cheek. When the subject's head was positioned comfortably, the imaging angle was set to 0° with respect to the camera optical axis in order to image the entire PWS while minimizing artifacts induced by facial curvature. All data were acquired in accordance with a protocol approved by the Institutional Review Board at University of California, Irvine.

Color Space Conversion

Image processing was performed with an algorithm previously described in studies using tristimulus colorimeters

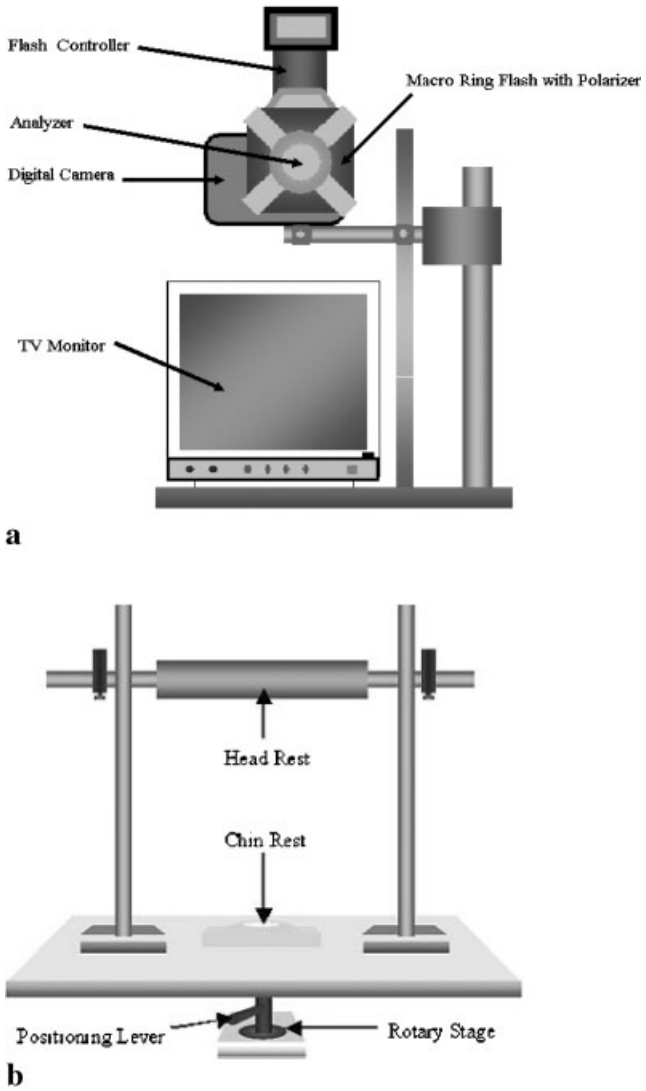

Fig. 2. (**a**) Diagram of the cross-polarized diffuse reflectance imaging system and (**b**) schematic of the head positioning device used to standardize images obtained from each subject.

[24,25]. To determine objectively skin color, the RGB color space of each image was converted to the CIE L*a*b* color space. To convert RGB images to CIE L*a*b* images, RGB values for each camera pixel were first converted into device-independent CIE XYZ tristimulus values using a conversion matrix (Equation 1) to transform images as if they were acquired under average daylight illumination at a standardized blackbody temperature of 6,500 K (Fig. 3):

$$\begin{bmatrix} X \\ Y \\ Z \end{bmatrix} = \begin{bmatrix} 0.412453 & 0.357580 & 0.180423 \\ 0.212627 & 0.715160 & 0.072169 \\ 0.019334 & 0.119193 & 0.950227 \end{bmatrix} \begin{bmatrix} R \\ G \\ B \end{bmatrix}. \quad (1)$$

To arrive at a set of XYZ values, two RGB images were required: (1) a raw RGB image of skin and (2) an image of a

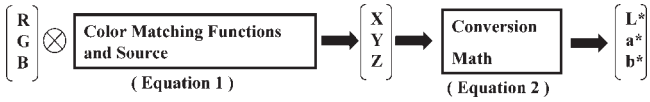

Fig. 3. Diagram of procedure used to convert RGB images to CIE L*a*b* images. Equation 1 and 2 are described in the text.

99% diffuse reflectance plate (Model SRT-99-100, Labsphere, North Sutton, NH). From these images, two XYZ tristimulus images were computed, one for skin (X, Y, Z) and the other for the calibration reference (X_n, Y_n, Z_n). The final step was to convert the skin XYZ images into CIE L*a*b* color images using the following equations:

$$\begin{aligned} L^* &= 116 \times (Y/Y_n)^{1/3} - 16 \quad \text{for } Y/Y_n > 0.008856 \\ L^* &= 903.3 \times (Y/Y_n) \quad \text{otherwise} \\ a^* &= 500 \times [f(X/X_n) - f(Y/Y_n)] \\ b^* &= 200 \times [f(Y/Y_n) - f(Z/Z_n)] \end{aligned} \quad (2)$$

where $f(t) = t^{1/3}$ for $t > 0.008856$
$f(t) = 7.787 \times t + 16/116$ otherwise.

Image Analysis

Custom software written in MATLAB (version 6.1, The MathWorks, Natick, MA) was used for image analysis. Using Equation 1 and 2, an acquired RGB image including both normal and PWS skin was converted to CIE L*a*b* color images. A relative a* index difference (Δa*) image was

Fig. 4. Image of port wine stain (PWS) skin taken without use of crossed polarizers. Image information is corrupted by specularly reflected light.

computed using the following equation:

$$\Delta a^* = \left[\left(a^*_{Pws} - a^*_{Ns}\right)/a^*_{Ns}\right] \times 100 \quad (3)$$

where a^*_{Pws} represents the a* index of PWS skin and a^*_{Ns} is the average a* index of normal skin. Thus, Δa^* represents the relative difference in erythema of PWS skin as compared to that of normal skin at each pixel (Table 2).

RESULTS

Cross-Polarized Diffuse Reflectance Imaging of PWS Skin

A comparison of PWS skin acquired without (Fig. 4) and with (Fig. 5) crossed polarizers demonstrates the effect of specular reflectance on image quality. The image shown in Figure 4 was taken with a commercial digital camera (Model Coolpix995, Nikon Co., Tokyo, Japan) under ambient room lighting conditions. The specular reflectance, apparent as glare in Figure 4, overwhelms color information evident in the absence of glare (Fig. 5a,b). Using the 99% diffuse reflectance plate, the average RGB values of the acquired diffuse reflectance were calculated as 251.7, 253.7, and 252.1, respectively, with standard deviations of ~1. To test system repeatability, images of the same 99% diffuse reflector were acquired on five different days. RGB values (mean ± standard deviation) were 250 ± 1.3, 252 ± 1.7, and 251 ± 1.2, respectively, demonstrating the stability and reproducibility of our imaging system.

a* and L* Index Images

Utilizing the procedure diagrammed in Figure 3, cross-polarized RGB images of the patient's PWS (Fig. 5a,b) were transformed to the CIE L*a*b* color space. Figures 6 and 7 are a* and L* index images, respectively, derived from the RGB image acquired before laser treatment (Fig. 5a). The color bars in Figures 6 and 7 denote quantitative measures of skin erythema and melanin content, respectively. Higher a* values denote more pronounced PWS skin erythema. A value of 0 in Figure 6 denotes complete absence of erythema. Higher L* values in Figure 7 denote low melanin content.

Relative Difference a* Index Image

To demonstrate the relative degree of erythema in PWS versus normal skin, Δa^* images were computed. The three different regions outlined as boxes by solid red lines in Figure 8 were selected as representative normal skin. Average normal skin values a^*_{Ns} of before and after laser treatment images (Fig. 8a,b, respectively) were 6.61 ± 0.56 and 5.55 ± 0.23, respectively. After laser treatment, Δa^* values were reduced as compared to corresponding PWS

Fig. 5. Cross-polarized diffuse reflectance RGB image of the same patient shown in Figure 4, taken (**a**) before and (**b**) after pulsed dye laser (PDL) treatment. Dashed black lines denote area used in subsequent analysis (see Fig. 9).

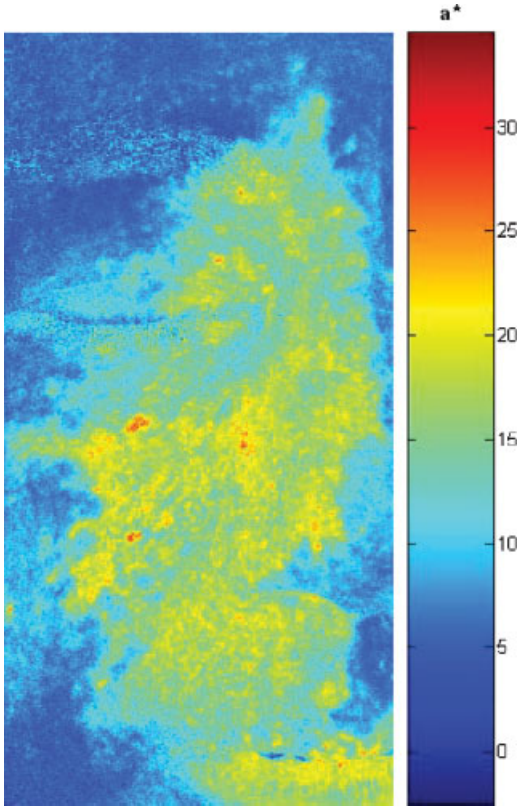

Fig. 6. a* Index image calculated from Figure 5a. This image shows that the PWS region consists of a* values typically greater than ~10. Maximum range of a*values is −60 (green) to +60 (red).

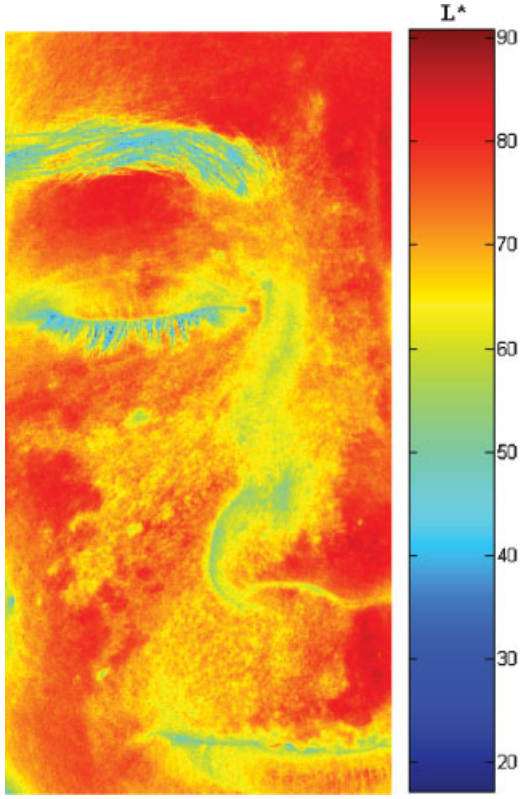

Fig. 7. L* index image calculated from Figure 5a. A higher L* value indicates lower melanin content. Maximum range of L* values is 0 (black) to 100 (white).

areas before treatment. For example, average Δa* values in the selected region numbered 1, 2, and 3 in Figure 8a were 186.5, 163.4, and 148.37%, respectively. However, after treatment, the average Δa* in the identical regions in Figure 8b were reduced to 125.4, 122.2, and 122.5%, respectively, due to the expected blanching of the PWS in response to laser therapy.

Erythema Distribution in a* Images

From the RGB image shown in Figure 5a, a predefined region marked by dotted black lines was selected and presented in Figure 9a. Even with a close up view of this region, it is difficult to identify distinct regions of high or low erythema. In the corresponding a* index image (Fig. 9b), contrast is substantially enhanced. This illustrates the benefit of employing this index, which can be used to distinguish between regions of high and low erythema that would otherwise be much less obvious.

DISCUSSION

An advantage of our cross-polarized diffuse reflectance imaging system is the use of polarization optics to remove glare. When light is incident on skin, ~5% is reflected due to the refractive index mismatch between human skin and air. Such specularly reflected light contains information on the superficial texture of the skin surface. However, specular reflectance impairs observation of skin color information provided by light scattered and absorbed from subsurface structures. Thus, an image of skin taken without crossed polarizers (Fig. 4) contains information on surface morphology (in the form of specular reflectance), and skin pigmentation and degree of vascularization (in the form of diffuse reflectance). Since specularly reflected light is in the same polarization state as incident light, crossed polarizers were used to remove unwanted specular reflectance, resulting in images containing primarily subsurface information on skin chromophore content (Fig. 5).

For objective PWS characterization, RGB values of cross-polarized images (Fig. 5) were converted to the device-independent CIE L*a*b* color space (Figs. 6 and 7), allowing for comparison of images taken under different experimental conditions. This conversion permits an objective comparison of our approach against commercial devices such as tristimulus colorimeters and reflectance spectrophotometers. We hypothesize that our system can provide similar information to these devices, and future studies will involve a quantitative comparison of both approaches.

Examination of an a* index image (Fig. 6) provides quantitative information on PWS skin color. Contrast in

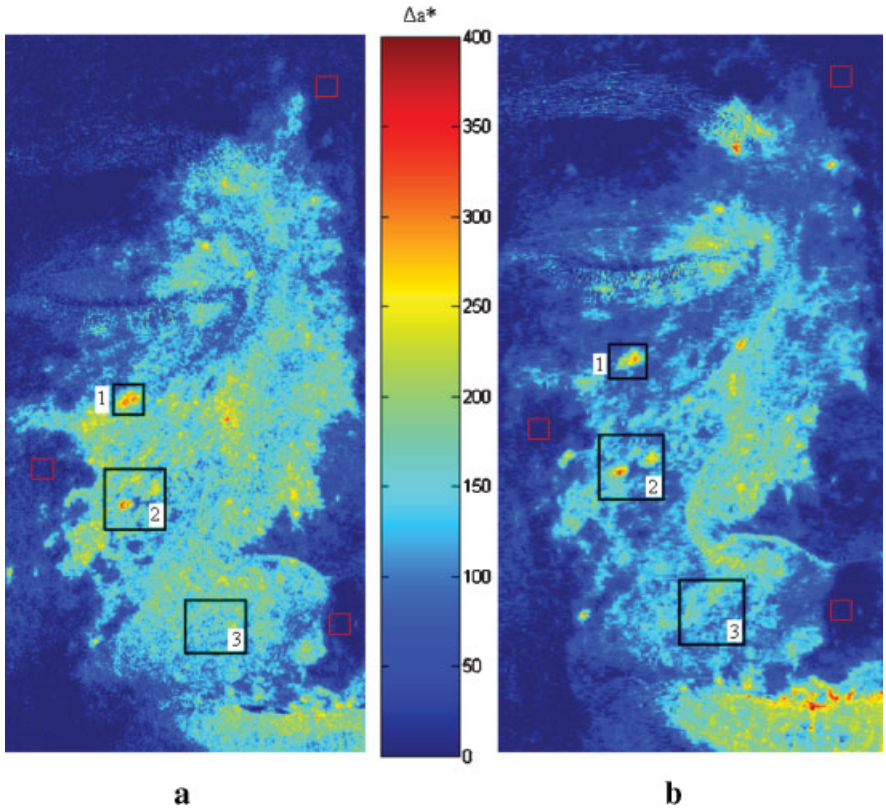

Fig. 8. Relative a* Index difference (Δa*) images (**a**) before and (**b**) after laser treatment images shown in Figure 5a and b, respectively. The solid red lines in each image denote regions selected as normal skin and used in calculation of Δa*.

this image is greater than that shown in the cross-polarized image (Fig. 5a). Previous studies have demonstrated that the a* index is a reliable indicator of skin erythema, which is related to local blood concentration [14,15]. Shriver et al. [12] have shown that a* values are affected by epidermal melanin content. With high melanin content, the a* value is not related solely to hemoglobin content due to high absorption of green light by melanin. Since negative values of a* represent the relative "greenness" of an object, substantial filtering of green light by melanin may significantly affect a* values. In the images of the PWS patient under study, the a* (Fig. 6) and the L* (Fig. 7) index images demonstrated that high values of a* (i.e., high degree of erythema) occurred in regions with relatively low L* (i.e., high melanin content). However, this negative correlation between a* and L* is not expected for all PWS patients. We are currently investigating the use of correction factors to reduce the impact of epidermal melanin content on a* values.

Our image analysis system can be applied to quantitate PWS blanching after laser treatment. Ideally, the degree of erythema should be decreased with each successive treatment. To observe the blanching effect, an a* index image can be computed prior to each successive laser treatment and compared to previous images. However, by using only an a* index image for comparison, determination of treatment efficacy may be inaccurate because of variations in skin pigmentation between subsequent images. In order to solve this problem, the relative degree of erythema before and after laser treatment was computed in PWS and compared to normal skin (Fig. 8). The selected normal skin sites were denoted by solid red lines in Figure 8 and chosen at flat sites proximal to the PWS. Multiple normal skin regions were evaluated to reduce artifacts caused by vertical and horizontal patient movement offset. In the Figure 8, a* indices of PWS skin erythema after laser treatment (Fig. 8b) were less than pre-treatment values (Fig. 8a) due to the expected PWS blanching in response to therapy. For examples, average Δa* values of the selected region 1, 2, and 3 before laser treatment were 186.5, 163.4, and 148.37% higher than that of normal skin, respectively. However, after laser treatment, the average Δa* in the same regions were reduced to 125.4, 122.2, and 122.5%, respectively, as compared to the normal skin. Studies are underway to investigate the efficacy of our imaging system for objective evaluation of PWS blanching throughout an extended treatment protocol.

Examination of a close up view of PWS skin (Fig. 9a) shows a diffuse red region, indicating erythema originating from subsurface blood vessels. As noted above, the a* index

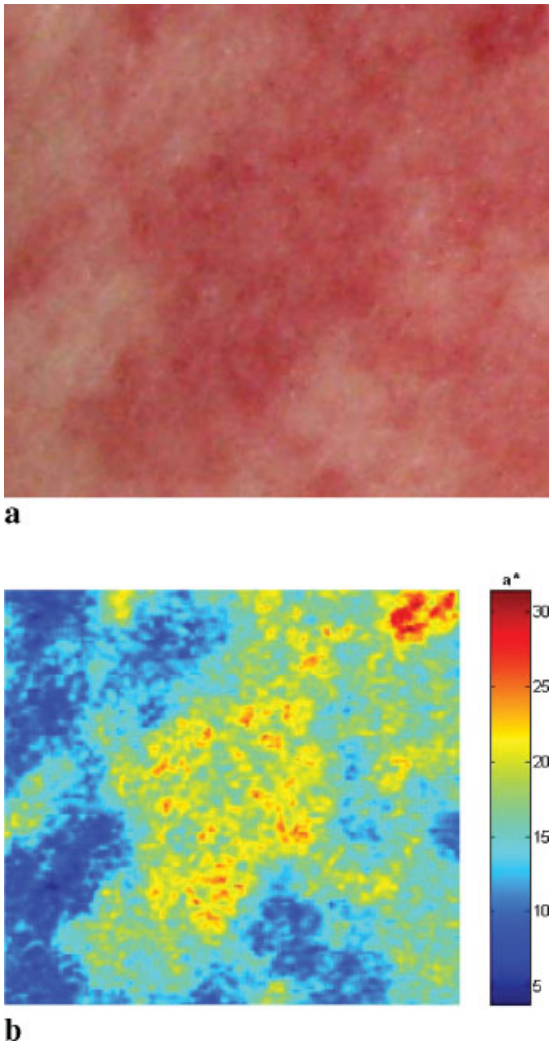

Fig. 9. (**a**) Cross-polarized diffuse reflectance image of a predefined region shown in Figure 5a. Subregions of high and low erythema are difficult to separate. (**b**) a* Index image of (a). Image contrast is improved substantially, allowing for clear visualization of regions of high and low erythema.

image is representative of local blood content. The corresponding a* index image (Fig. 9b) shows a more distinct blood vessel pattern with enhanced contrast as compared to the cross-polarized image (Fig. 9a). Experiments are planned to determine correlations between the blood vessel patterns in the a* index images and actual blood vessel distributions.

Although our imaging system offers many advantages over other devices, several issues need to be addressed for further optimization. Ideally, regions of interest should be oriented perpendicular to the camera; in reality, curved surfaces are present. The effect of curvature on image fidelity will be studied in future work, in which the light distribution on the sample surface as a function of angle will be measured and the effects on a* and L* index images investigated. Furthermore, user-friendly control for image analysis needs to be developed before routine clinical deployment.

In the present study, PWS skin was imaged with a cross-polarized diffuse reflectance imaging system. Image processing allowed determination of erythema (a*) and melanin content (L*) and might be an effective tool to document PWS blanching in response to laser therapy. Using this system, a relatively large area is imaged in a noncontact fashion, which is an advantage over point measurement systems such as reflectance spectrophotometry and tristimulus colorimetry. In addition, problems associated with conventional digital images such as glare, shadowing, and nonuniform illumination, were minimized. Finally, the head positioning device can alleviate problems caused by variations in positioning, measurement distance, and camera angle.

REFERENCES

1. Nelson JS, Kelly KM, Zhao Y, Chen Z. Imaging blood flow in human port-wine stain in situ and in real time using optical Doppler tomography. Arch Dermatol 2001;137:741–744.
2. Onizuka K, Tsuneda K, Shibata Y, Ito M, Sekine I. Efficacy of flashlamp-pumped pulse dye laser for port wine stains: Clinical assessment and histopathological characteristics. Br J Plast Surg 1995;48:271–279.
3. Koster PHL, van der Horst CMAM, Bossuyt PMM, van Gemert MJC. Prediction of portwine stain clearance and required number of flashlamp pumped dye laser treatments. Lasers Surg Med 2001;29:151–155.
4. Michel S, Landthaler M, Hohenleutner U. Recurrence of port-wine stains after treatment with the flashlamp-pumped pulsed dye laser. Br J Dermatol 2000;143:1230–1234.
5. Tan OT, Sherwood K, Gilchrest BA. Treatment of children with port-wine stains using the flashlamp-pulsed tunable dye laser. New Engl J Med 1989;320:416–421.
6. Haederdsal M, Efsen H, Gniadecka M, Fogh H, Keiding J, Wulf HC. Changes in skin redness, pigmentation, echostructure, thickness, and surface contour after 1 pulsed dye laser treatment of port-wine stains in children. Arch Dermatol 1998;134:175–181.
7. van Gemert MJC, Nelson JS, Milner TE, Smithies DJ, Verkruysse W, de Boer JF, Lucassen GW, Goodman DM, Tanenbaum BS, Norvang LT, Svaasand LO. Noninvasive determination of port wine stain anatomy and physiology for optimal laser treatment strategies. Phys Med Biol 1997; 42:937–950.
8. Le KT, Shahidullah H, Frienden IJ. Review of modern techniques in detecting port-wine stain response to laser therapy. Dermatol Surg 1999;25:127–132.
9. Trolius AM, Ljungren B. Reflectance spectrophotometry in the objective assessment of dye laser-treated port-wine stains. Br J Dermatol 1995;132:245–250.
10. Trolius AM, Ljungren B. Evaluation of port wine stains by Laser Doppler perfusion imaging and reflectance photometry before and after pulsed dye laser treatment. Acta Derm Venereol 1996;76:291–294.
11. Berardesca E, Elsner P, Wilhelm K-P, Maibach HI. Bioengineering of the skin: Methods and instrumentation. Boca Raton, FL: CRC Press. 1995:29–40.
12. Shriver MD, Parra E. Comparison of narrow-band reflectance spectroscopy and tristimulus colorimetry of measurements of skin and hair color in persons of different biological ancestry. Am J Phys Anthropol 2000;112:17–27.
13. Takiwaki H, Shirai S, Kanno Y, Watanabe Y, Arase S. Quantification of erythema and pigmentation using a video-microscope and computer. Br J Dermatol 1984;131:85–92.
14. Clarys P, Alewaeters K, Lambrecht R, Barel AO. Skin color measurements: Comparison between three instruments: The

Chromameter, the DermaSpectrometer and the Mexameter. Skin Res Technol 2000;6:230–238.
15. Alaluf W, Atkins D, Barrett K, Blount M, Carter N, Heath A. The impact of epidermal melanin on objective measurements of human skin color. Pigment Cell Res 2002;15:119–126.
16. Barel AO, Clarys P, Alewaeters K, Duez C, Hubinon JL, Mommaerts M. The Visi-Chroma VC-100: A new imaging colorimeter for dermatocosmetic research. Skin Res Technol 2001;7:24–31.
17. Takiwaki H, Miyaoka Y, Skrebova N, Kohno H, Arase S. Skin reflectance-spectra and colour-value dependency on measuring-head aperture area in ordinary reflectance spectrophotometry and tristimulus colourimetry. Skin Res Technol 2002; 8:94–97.
18. Wagner JK, Jovel C, Norton HL, Parra EJ, Shirver MD. Comparing quantitative measures of erythema, pigmentation and skin response using reflectometry. Pigment Cell Res 2002;15:379–384.
19. Takiwaki H, Miyaoka Y, Kohno H, Arase S. Graphic analysis of the relationship between skin colour change and variations in the amounts of melanin and hemoglobin. Skin Res Technol 2002;8:78–83.
20. Seraro M, Sparavigna A. Quantification of erythema using digital camera and computer-based image analysis: A multicentre study. Skin Res Technol 2002;8:84–88.
21. Young-Gee SA, Kurwa HA, Barlow RJ. Objective assessment of port-wine stains following treatment with the 585 nm pulsed dye laser. Aust J Dermatol 2001;42:243–246.
22. Miyamoto K, Takiwaki H, Hillebrand GG, Arase S. Utilization of a high-resolution digital imaging system for the objective and quantitative assessment of hyperpigmented spots on the face. Skin Res Technol 2002;8:73–77.
23. Rah DK, Kim SH, Lee KH, Park BY, Kin DW. Objective evaluation of treatment effects on port-wine stains using L*a*b* color coordinate. Plast Reconstr Surg 2001;108:842–847.
24. Haeghen YV, Naeyaert JMAD, Lemahieu I. An imaging system with calibrated color image acquisition for use in dermatology. IEEE Trans Med Imaging 2000;19:722–730.
25. Malacara D. Color vision and colorimetry: Theory and applications. Bellingham, WA: SPIE Press. 2002:90–101.